Research Article | Vol. 10, No. 3 | 1 Mar 2019 | BIOMEDICAL OPTICS EXPRESS 1351
Biomedical Optics EXPRESS

Optical fiber technology enables smart needles for epidurals: an *in-vivo* swine study

Benito Carotenuto,[1] Armando Ricciardi,[1,3] Alberto Micco,[1] Ezio Amorizzo,[2] Marco Mercieri,[2] Antonello Cutolo,[1] and Andrea Cusano[1,4]

[1]*Optoelectronics Group, Engineering Department, University of Sannio, Benevento I-82100, Italy*
[2]*Pain Medicine Unit, Sant'Andrea Hospital, "Sapienza" University, Rome I-00189, Italy*
[3]*aricciardi@unisannio.it*
[4]*a.cusano@unisannio.it*

Abstract: Nowadays, epidural space identification is made by using subjective and manual techniques characterized by failure rates up to 7%. In this work, we propose a fiber optic sensor technology based needle guidance system, that is directly inspired by the most common technique currently used for epidurals; through real-time strain measurements, the fiber Bragg grating integrated inside the needle lumen is able to effectively perceive the typical force drop occurring when the needle enters the epidural space. An *in vivo* swine study demonstrates the validity of our approach, paving the way for the development of lab-in-a-needle systems.

1. Introduction

Epidural anesthesia (EA) is the most common loco-regional anesthesia practice used for labor, postoperative and chronic pain treatment [1]. Basically, the medical procedure for EA consists in inserting a needle into the skin and directing it towards the epidural space (ES) where the anesthetic is injected. The ES is located in the spine, between the ligament flavum and the dura. Currently, the correct placement of the needle tip into ES is determined by exploiting 'manual techniques', including the most common Loss of Resistance (LOR). LOR technique consists in advancing the needle by applying constant or intermittent pressures to a specific syringe plunger. Once the needle crosses the ligament flavum (which is a hard tissue), an abrupt resistance drop on the plunger is perceived. Despite the simplicity, LOR is a 'blind' technique and the success of this procedure depends on the expertise of the operator. Failures occur up to 7% of the cases, and typically causes dura perforation with complications to both the patient (severe headache and backache) and healthcare system (lengthened hospitalization) [2]. Although accurate imaging procedures such as fluoroscopy or CT are often used in Pain Medicine, their use in routine clinical anesthesia is unpractical and expensive.

The demand for reliable and safe procedures for EA is continuously promoting the exploration of novel technological solutions [3]. In the last decade, pump-based electronic systems [4,5], ultrasounds [6,7] and optical devices [8–11] have been proposed. Specifically, optical devices exploit the unique properties of optical fibers (biocompatibility, lightweight, high aspect ratio) that are integrated inside epidural needles and catheters. By doing so, guidance systems based on refractometry and Optical Coherence Tomography (OCT) have been reported. Refractometers basically consist of fibers that measure the absorption spectra of the tissues penetrated by the needle [8]. ES is localized thanks to the presence of specific absorption wavelengths relative to fat and blood. On the other hand, OCT devices use optical fibers to collect high-resolution images during needle advancement in order to differentiate among different tissues [9–11]. None of the approaches proposed so far allow to reach the

#331554 https://doi.org/10.1364/BOE.10.001351
Journal © 2019 Received 14 May 2018; revised 18 Dec 2018; accepted 14 Jan 2019; published 21 Feb 2019

Biomedical Optics EXPRESS

required degree of accuracy and specificity necessary to replace the existing techniques and become the new gold standard for EA.

In this scenario, we have recently proposed an optical guidance system, which combines the principle of operation of the LOR technique with the advantages offered by the optical fiber sensor technology. Our system is based on a special coated fiber Bragg grating (FBG) directly integrated inside the lumen of the epidural needle.

FBG based strain and force sensors have been widely used in medical applications [12]. In particular, FBGs have been developed and integrated into robotics [13], endoscope [14] and needle [15,16] for shape detection. These optical fiber-based needles, being inherently immune from interference induced by surrounding electromagnetic fields, are particularly useful in the applications involving magnetic resonance imaging systems [17–20].

In our specific application, the FBG detects in real time the consistency of the tissues encountered by the needle during penetration by means of strain measurements. The proof-of-principle demonstration in a training phantom tissue was recently reported [21]. In this work, with the aim of evaluating the extent to which 'real tissue' heterogeneity influences the device performances, we report on the results of an *in vivo* swine study carried out by using two optical probes with different external coating material. Albeit preliminarily, experimental results reveal that our device has the potential to improve the accuracy of ES identification, thus making objectified what is currently at the clinician's discretion.

2. Materials and methods

2.1 Fiber Bragg grating probes

The FBG is a well-known optical fiber sensor that is used in a vast range of applications [22]. The FBG is manufactured by imprinting with UV light a 1D periodic grating (i.e. a refractive index modulation) along the fiber photosensitive core, for a distance of a few millimeters. The grating period Λ and the effective refractive index n_{eff} determine the Bragg wavelength $\lambda_B = 2n_{eff}\Lambda$; when the wavelength of the light propagating into the FBG is equal to λ_B, the whole power is reflected, otherwise it is transmitted. External solicitations modifying both Λ and n_{eff}, such as temperature or strain variations, cause the shift of λ_B; this basically represents the sensing mechanism of FBG. In our study, the FBGs were provided by FBGS international (Belgium); they were fabricated by using the draw-tower process with a standard single mode optical fiber [23]. Specifically, two FBG coated with different elastometers were used to enhance the strain sensitivity (a schematic view of the cross section is shown in Fig. 1(a).). The first FBG is coated with Hytrel [24]. Thin layers of ormocer and silicone are used as buffer layers to increase the adhesion. Although unique properties of Hytrel make it ideal for devices requiring a balance of flexibility and compactness, its use in medical application is mostly limited to cases not involving implantation in the human body [25]. The second FBG, instead, is coated with PEEK, a thermoplastic polymer characterized by an excellent biocompatibility [26]. Due to its properties, PEEK is typically exploited for *in vivo* medical devices used for skull replacement in neurosurgical applications, spinal fusion orthopedics implant, dentures, just to name a few [27].

The Hytrel (PEEK) coated FBG has a Bragg wavelength of 1557.7 nm (1543.6 nm), a FWHM of ~190pm (~320pm) and a peak reflectance of −13.8 dB (−24 dB). Both the FBGs are 8mm long.

Biomedical Optics EXPRESS

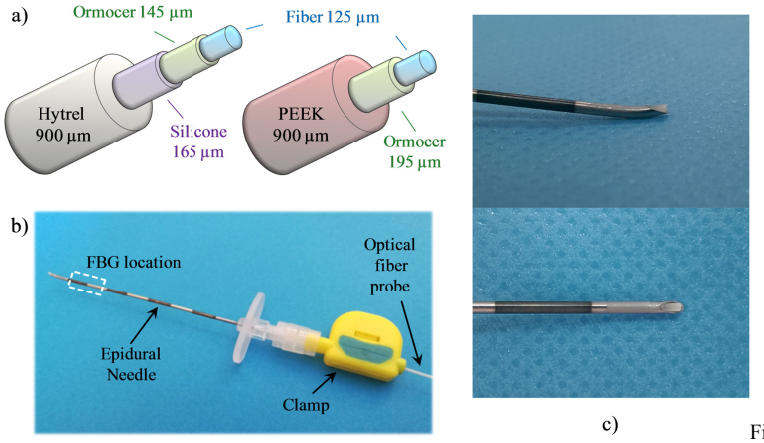

Fig. 1. Schematic view of the (a) Hytrel coated- and PEEK coted- probes illustrating the layers thicknesses; (b) Picture of our device where the probe is integrated in the Tuohy needle and locked to it by means of a clamp; (c) close-up of the needle tip integrated with the HCP.

Coated FBG are integrated inside the lumen of a standard 18-gauge Tuohy needle (Fig. 1(b)). To this aim, both the probes have been fabricated with an overall outer diameter of 900 µm in order to fit the needle lumen size (diameter ~1.03 mm). Therefore, the strain exerted on the FBG is almost entirely on axis because the FBG bending inside the needle lumen is avoided. The fiber probe–needle integration procedure has been already discussed in our previous work [21]. Specifically, the needle is placed orthogonally to a reference plane; then the optical fiber probe is inserted inside the needle until it goes in touch with the plane. The insertion process is stopped in correspondence of a total compressive pre-strain equivalent to a Bragg wavelength shift of 10pm. At that point, the optical fiber probe is locked with the clamp, and the system is ready to use. Once completed that procedure, the fiber probe comes out of the needle rounded tip (see Fig. 1(c)). When the clamp is opened, the probe can be easily pulled off the needle.

2.2 Console

To interrogate the FBG the Micron Optics sm130 was used. This commercial FBG interrogator comprises a swept laser source sending light in the wavelength range of 1510-1590nm, and a photodiode collecting the reflected signal; a highspeed hardware peak detection tracks the resonance wavelength changes as a function of time. In this study, a sampling rate of 1kHz was used during all tests. We implemented a customized Labview plug-in for visualizing and recording in real time the Bragg wavelength shifts. Signal processing was performed offline, with scripts written in Matlab R2009b.

2.3 Calibration tests

Calibration tests were carried out to correlate the wavelength shifts and the force applied on the probe tip. For this purpose, a custom setup was assembled in our laboratory (see. Figure 2(a)). This setup comprises two parts: the base supporting a metallic spindle and a customized syringe/needle device in which the optical fiber probes are inserted. The base is an arrangement of 3 rectangular nylon slabs that are spaced apart from each other by means of 4 metallic pillars; at the center of each guide there is a hole of 1.2mm in diameter where the needle is free to slide. In the bottom slab, in correspondence of the center, there is a metallic spindle with diameter of 900µm. The modified syringe is equipped with a container for small weights and it is connected to the 18-gauge needle. For this test only, the presence of the syringe excludes the use of the clamp, so that the fiber probe is glued in the luer connector of the syringe, in correspondence of the distal end of the needle. Basically, the glue, that is used

Biomedical Optics EXPRESS

only for the calibration setup, replaces the function of the clamp that, instead, is used in all the other tests including *in vivo* measurements. By inserting the syringe/needle device into the base, the probe goes in contact with the spindle, thus involving a compression of the FBG. Therefore, by applying a known weight force, the FBG pushes on the spindle and the relative Bragg wavelength shift is measured. The calibration curves obtained for the Hytrel coated probe (HCP) and the PEEK coated probe (PCP) are shown in Fig. 2(b). Both the probes exhibit a linear response in the force range 0-2 N; the R^2 coefficients for HCP and PCP curves are 0.998 and 0.999 respectively. Specifically, HCP showed a sensitivity (–554 pm/N) about 1.5 times higher than the PCP (–363 pm/N). Higher sensitivity of HCP is mainly due to the lower equivalent Young modulus characterizing this sensor (1.7GPa, see [21] for details) with respect to the PCP (4.8 GPa). The slight discrepancy between the Young moduli ratio (~2.8) and sensitivity ratio (~1.5) of the two probes could be due to their different strain transfer mechanism of the multilayer coating structure.

The linear relationship between the wavelength shift and the applied force (Fig. 2(b)) demonstrates that the measured deformation is mainly a compression of the FBG along the fiber axis as compared to a tilt. Moreover, since the fiber probe is not glued inside the needle lumen, the needle bending does not influence the FBG response. To demonstrate that, we have fixed the needle at one distal end, and then we have created a bending with a tilt angle of ± 15 degrees, as described in Fig. 2(c). Note that for this test, the fiber probe is mechanically locked at the needle through the clamp. The Bragg wavelength was monitored at each bending angle for 1 second. The average values of 1000 samples are shown in Fig. 2(d); the Bragg wavelength variations are in the interrogator noise levels range (Fig. 2(d)).

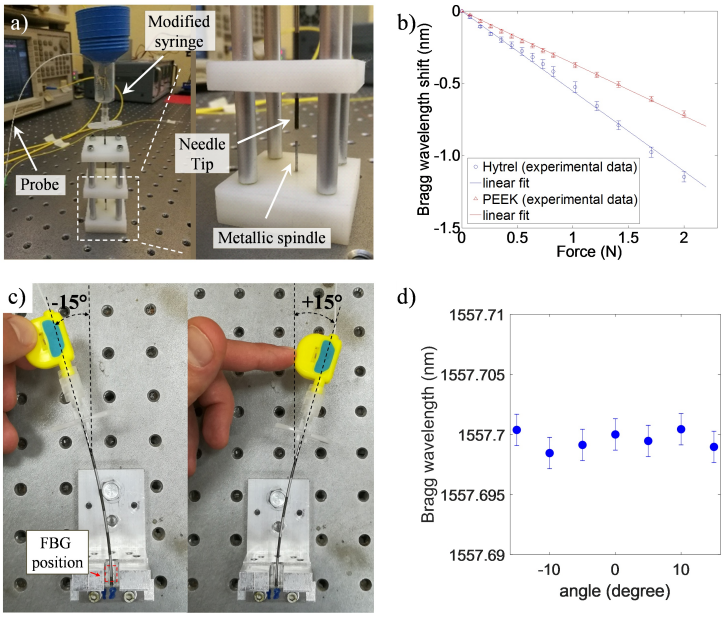

Fig. 2. (a) The calibration setup; a close-up (figure inset) of the base showing the metallic spindle (b) Calibration curves of HCP (blue) and PCP (red); (c) setup for the tilt test. (d) Bragg wavelength as a function of the bending angle registered with the HCP.

2.4 Experimental methodology

Experiments were authorized by Italian Ministry of Health (auth. N. 554/2017) and carried out at Cardarelli Hospital in Naples (Italy). A female pig (age 7 months, weight 70kg) was anesthetized with an intrevenous injection of propofol 2 mg/kg, vecuronium 0.1 mg/kg, fentanyl 0.03mg/kg and maintained with propofol infusion 4 mg/Kg/h, Ketamine 0.5

Biomedical Optics EXPRESS

mg/kg/h. The pig was intubated, mechanically ventilated and was laid in prone position. Continuous monitoring of heart rate, pulse oximetry and blood pressure were carried out throughout the experiment. The pig was euthanized after the procedure.

Six needle insertions were manually performed by a skilled clinician. Needles integrated with both HCP and PCP were inserted into L5/L6, L6/L7 and L7/S1 interlaminar spaces by following a midline approach. The Bragg wavelength values were measured in real-time during the needle advancement. The procedure starts by inserting the sensorized needle into the connective tissue, where it is left until the thermal stabilization of the Bragg wavelength is achieved. In fact, the gradient between the room temperature (~20°C) and the animal internal temperature (~37°C) causes a Bragg wavelength drift. Stabilization time is no longer than 10 seconds. Further temperature variations inside the body are estimated to be less than 1°C, and thus the cross-sensitivity effect with respect to strain is negligible. Moreover, temperature variations induce Bragg wavelength shifts that are significantly slower than those associated to strain changes. Therefore, if necessary, the temperature effects can be easily filtered out in the signal post processing. Then, the needle is advanced toward the ES until an abrupt Bragg wavelength red-shift (force drop) preceded by a minimum dip (force peak) occurs. This event is the analogue of the loss-of-resistance that physicians experience on their syringe when the ligamentum flavum is penetrated and the needle enters the ES. In all the experiments, correct identification of ES was confirmed by X-ray imaging.

3. Results

3.1 Test with the Hytrel probe

Figure 3(a) shows the force variation as a function of time measured by HCP during needle advancement into L7/S1 space. The horizontal gray line represents the baseline (meaning no force applied) and it is set at the end of the above mentioned thermal stabilization phase. The baseline is set once the needle is inserted into the pig back, when the pushing force exerted by the clinician is zero. As the probe slightly protrudes from the needle tip, the FBG is always compressed when being inserted inside the tissue. The baseline is taken every time the single procedure starts, and it differs from case to case. Therefore, each single measurement is self-referenced, so that cross-sensitivity effects do not influence our measurements.

Biomedical Optics EXPRESS

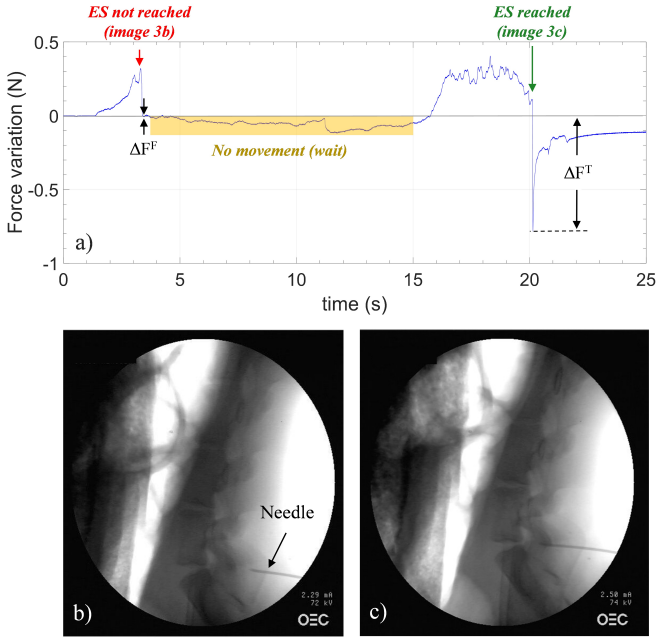

Fig. 3. (a) Force variations versus time measured by HCP in L7/S1; gray line represents the baseline (details in the text). X-ray images captured for monitoring the needle position during advancement: (b) wrong and (c) correct positioning of the needle.

When the needle was advanced, a positive force variation was measured, followed by a force drop (marked with a red arrow) occurring at about 3 seconds. At that point, the needle advancement was stopped and an X-ray image was captured. This image, shown in Fig. 3(b), demonstrates that the needle tip is far away from the ES, and it is presumably close to the ligamentum flavum. Needle advancement restarted at ~15 seconds; the force increased again, due to ligamentum flavum stiffness, until another abrupt drop (marked with a green arrow) occurred at ~20 seconds. When the needle crosses the ligament flavum, it enters the ES, inducing a fast relaxation of the probe and thus a force drop. The X-ray image captured at that point (Fig. 3(c)) confirmed that the needle entered the ES. Note that the signal variation registered between 3 and 15 seconds in Fig. 3(a) is not due to any temperature effect, but it is related to the fact that, after perceiving the drop, the clinician released the grip on the needle and stopped applying a pulling force. In doing so, the FBG undergoes less strain until the needle insertion restarts.

Biomedical Optics EXPRESS

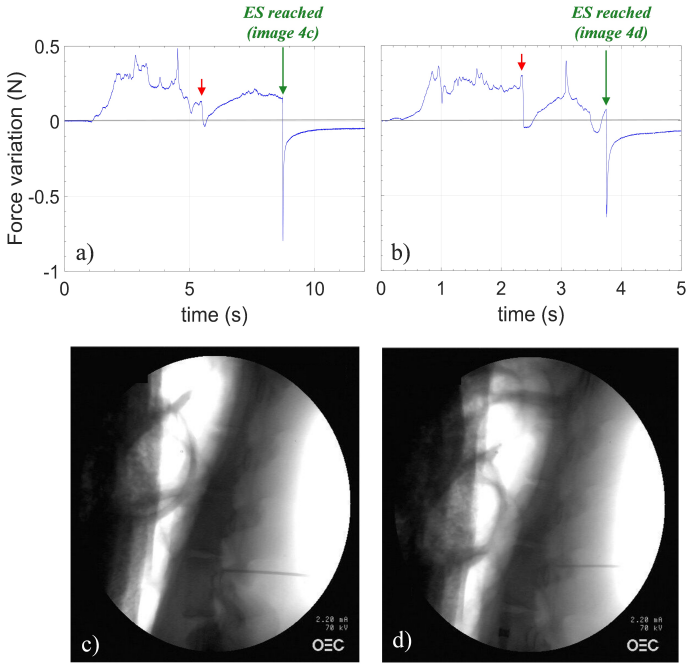

Fig. 4. Force variations versus time measured by HCP in (a) L6/L7 and (b) L5/L6; gray line represents the baseline (details in the text). X-ray images captured afterward the correct positioning of the needle in ES in (c) L6/L7 and (d) L5/L6.

Figures 4(a) and 4(b) show the force variations as a function of time measured by HCP during needle advancement into L6/L7 and L5/L6 space respectively. In these two cases, the needle was continuously advanced toward the ES without interruption. All the punctures were performed manually, meaning that advancing rate is not the same in all tests. Although the penetration time for each puncture is different, some common distinctive features appear. In fact, by directing the sensorized needle toward the ES, the compression force experienced by the probe deviates from the reference value. The force changes are directly related to the consistence of the tissues facing the probe during penetration. Specifically, when the stiffness of the tissues raises/decreases, the probe undergoes a compression/expansion, corresponding to a force increase/decrease. Red and green arrows in Fig. 4 indicate the force drops measured when the needle tip is immediately before and after the ligamentum flavum respectively. X-ray images confirmed the correct achievement of ES in both cases (Figs. 4(c) and 4(d)).

Overall, during the entire procedure, different force drops occur. For example, with reference to Fig. 3(a), the force drop (ΔF^F~-0.013N) occurring at ~3 seconds could be erroneously interpreted as the entry into the ES; similar considerations also hold for the dip at ~5 seconds in Fig. 4(a). However, the mean value of force drops ΔF^T detected when the needle is correctly placed in the ES (−0,74 ± 0,09 N) is more than one order of magnitude higher than that detected with a wrong approach (−0.03 ± 0.02N).

3.2 The detection algorithm

To discriminate true from false events, a simple algorithm evaluating both speed and amplitude of negative force variations has been implemented. Specifically, the algorithm has the 3 following steps: (i) first, the force variations that are positive (i.e. larger than the baseline) are set to zero, (ii) then it is calculated the derivative of the signal resulting from step (i) and, finally (iii) it is evaluated the product of signals achieved in the steps (i) and (ii). The curves achieved during the elaboration process for the 3 punctures are reported in Fig. 5,

Biomedical Optics EXPRESS

where the 'raw' force variation (blue curves) are shown again for convenience. The processed signals exhibit unique peaks that are unequivocally associated to the ES entry. The peaks amplitude (0.17 ± 0.12 N^2/ms) is several orders of magnitude higher than the background ($1.23 \times 10^{-6} \pm 8.9 \times 10^{-5}$ N^2/ms). As shown in the inset of Fig. 5(d) the force drops take 5-10 ms, so that by sampling at 1KHz about 5-10 wavelengths are registered.

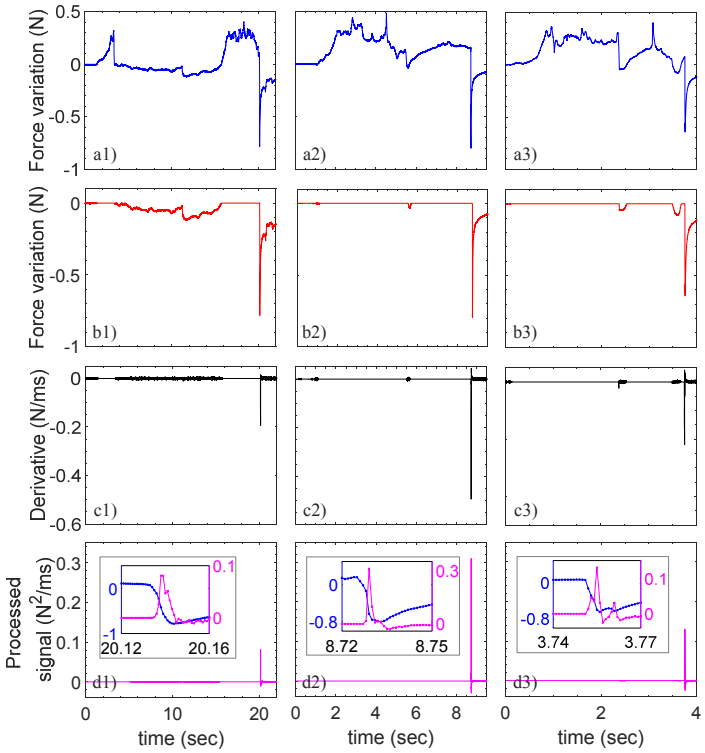

Fig. 5. Force variations measured by the Hytrel coated probes during penetration in L7/S1 (first column), L6/L7 (second column) and L5/L6 (third column) spaces: (a) original data; (b) the same of (a) where positive values are set to zero; (c) derivative of (b) ; (d) processed signal given by the multiplication between (b) and (c). The inset in (d) are the close-up images of (a) and (d) in correspondence of the force drops.

3.3 Tests with the PEEK probe

Figure 6 shows the force vs. time signal recorded with the second probe coated with PEEK (one puncture signal is shown as a representative example). In this case, it is possible to note from Fig. 6(a) that the probe provides very slow force variations (~0.08 N) which essentially results in a noisy flat derivative (Fig. 6(c)). By multiplying the curves of Figs. 6(b) and 6(c), the final processed signals becomes almost a constant zero line characterized by the absence of distinctive features. By comparing results of Fig. 5 and 6, it is worth noting that the relatively small difference in sensitivity (1.5 times lower than the HCP) makes a big difference in the force variation signals. This is due to the fact that, in the calibration procedure, the probes pressed against a metallic spindle that is a rigid body. Therefore, the force applied is totally transferred to the FBG, according to the stiffness of the external coating. However, during in vivo test, the probes press against a biological tissue that is, of course, an elastic and flexible body. As the stiffness/elasticity of PEEK is significantly higher/lower than that of Hytrel, during the needle advancement, while the HCP undergoes compression when it goes in contact with the biological tissues, the PCP, being characterized by a high compressive strength, remains rigid, and it pierce the tissue without undergoing

Biomedical Optics EXPRESS

significant compressions (meaning negligible wavelength shifts and thus negligible force variations).

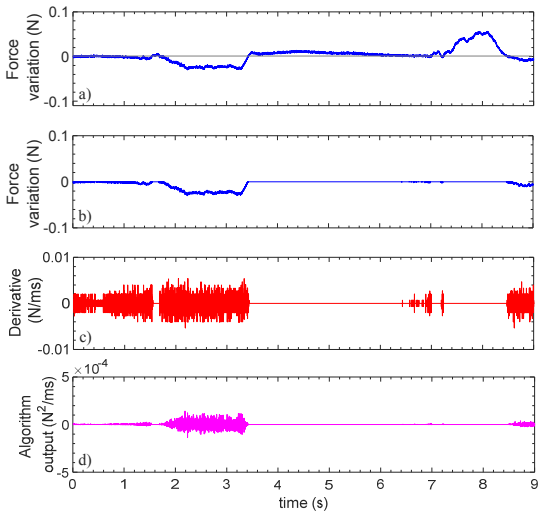

Fig. 6. Force variations measured by the PEEK coated probe during penetration in L5/L6 space: (a) original data; (b) the same of (a) where positive values are set to zero; (c) derivative of (b) ; (d) processed signal given by the multiplication between (b) and (c).

3.4 Study on the insertion speed

With the aim of demonstrating the ability of our probe to unequivocally identify the ES entry regardless of the operator-dependent insertion speed of the needle, we carried out further experimental tests. Specifically, we have assembled a benchtop setup, where the sensorized needle (i.e. the needle integrated with the FBG) is connected to a linear axis that can be advanced with controlled speed. The needle was pulled at different speed (in the range from 0.5 to 5 mm/s including the typical needle insertion speeds used in clinical practice) through a 4.5mm thick silicone-based tissue-mimicking phantom (shore hardness of 30A, corresponding to a Young module of about 1MPa). This kind of silicone membrane, produced by Smooth-On (https://www.smooth-on.com/tutorials/making-needle-insertion-trainer/), is widely used as a surrogate of tissues for clinical simulators [28]. Figure 7 shows the measured force variation as a function of time recorded during the advancement of the needle inside the silicone membrane at different speed values.

The raw signals exhibit two abrupt force drops due to the silicone membrane perforation (pointed out by arrows in Fig. 7(a)). However, by multiplying curves in Figs. 7(b) and 7(c), the algorithm filters out the spike related to positive force variations, so that only a unique peak remains in the processed signal shown in Fig. 7(d). There is a dependence of the maximum force value and the corresponding temporal derivative on the insertion speed. Specifically, the peak force and its derivative increase as the needle moves faster. These results clearly demonstrate that, for all the punctures, the processed signals provide unique and objectively distinguishable spikes as the needle overcomes the silicone membrane.

Biomedical Optics EXPRESS

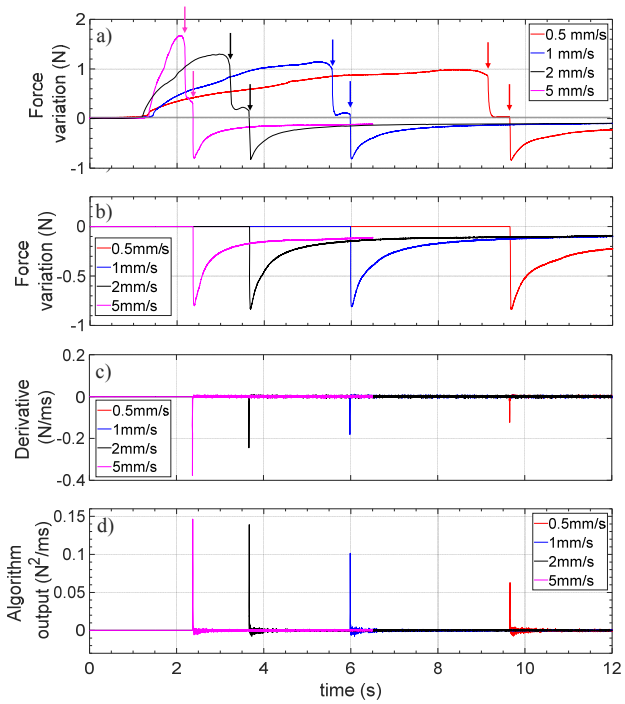

Fig. 7. Force variations measured by the Hytrel coated probe during the penetration of the silicone membrane at different penetration speeds: (a) original data; (b) the same of (a) where positive values are set to zero; (c) derivative of (b) ; (d) processed signal given by the multiplication between (b) and (c).

3.5 Analysis on the measurement uncertainty

Excluding the uncertainty due to the intrinsic variability of the human tissues, the main potential sources of error of our system in estimating the epidural space depth are related to the optical probe placement inside the needle, and to the insertion speed that is intrinsically operator dependent.

For evaluating the impact of these aspects on the sensor operation and related performances, we have repeated the study pertaining to the insertion speed with optical probes placed in different locations inside the needle. Specifically, by exploiting the integration procedure previously described in section 2.1, we have repeated the HCP integration 5 times achieving different pre-compressions corresponding to Bragg wavelength shifts in the range 8-12 pm. This is equivalent to a positioning error of the optical probe inside the needle of + –20% with respect to the reference value (10 pm). For each of the 5 different positioning configurations, the needle was pulled at 4 different speed (0.5, 1, 2 and 5 mm/s) through the silicone-based (ligamentum flavum mimicking) membrane mentioned in the previous section. For each puncture, we measured the time interval between the instant in which first sharp force drop starts to arise (trigger signal) and the appearance of peak in the algorithm output signal. This time extent corresponds to the temporal distance between the two arrows reported in Fig. 7. Basically, the first arrow indicates the point where the probe starts to relax but it is still in the compression state, and thus the needle tip is still inside the membrane. In other words, in this point, the probe is on the verge of crossing the membrane. Therefore, this point can be safely considered an over-estimation of the real time instant when the probe enters the target (epidural) space. The second arrow, instead, indicates the time instant provided by the algorithm, corresponding to the situation in which the needle tip is outside the membrane. Consequently, according to this conjecture, the time distance between

Biomedical Optics EXPRESS

the two arrows represents a conservative estimation of the epidural space identification uncertainty of our device, since it certainly include the time interval between the "real" and the "felt" arrival times of the needle tip within the target space.

In order to take into account the speed effects on the identification uncertainty, the evaluated time intervals have been converted in the spatial domain by multiplying them by the corresponding insertion speed. The results are summarized in Fig. 8 where we report the histogram of the calculated distances at each insertion speed. The values are represented as mean value ± one standard deviation that is of the order of 0.1-0.2 mm. It is possible to notice that the maximum error is achieved for high insertion speeds. It is important to consider that our measurements are also influenced by the variability of the membrane thickness that is measured to be 4.52 ± 0.21 mm.

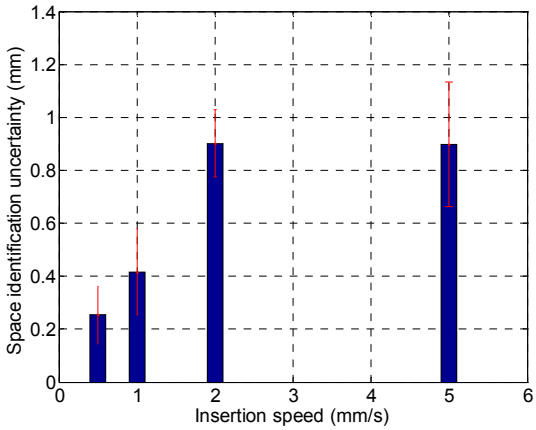

Fig. 8. Histogram of the distances between the two arrows of Fig. 7 (space identification uncertainty) as a function of the needle insertion speed. For each speed, the value is calculated as mean ± one standard deviation over 5 punctures made with different position of the HCP inside the needle (see the discussion in the text for further details).

In any case, we found that the maximum distance between the trigger signal and the algorithm peak registered in 20 punctures is less than 1.15 mm, and the overall space identification uncertainty (averaging all the measurements made) is 0.60 ± 0.35 mm. Now, considering that the epidural space depth (distance between the ligamentum flavum and dura mater) is typically in the range of 4-7mm in the mid-lumbar region, our device seems to correctly meet the need of placing the needle in position inside the space, avoiding the dura mater puncture. Other source of error due to the fabrication reproducibility of the optical probes are expected to not affect our measurements. In fact, nowadays, FBG fabrication procedures are well developed and they are ready for large scale production and use in industrial applications. Uncertainty of the optical sensing interrogator (SM130, Micron Optics) is 1 pm in the wavelength range from 1510 nm to 1590 nm, while the Bragg wavelength shift measured in our applications are in the order of hundreds of pm.

4. Discussion

Overall, the results achieved in this work confirm the guidance capability of our device envisaged in our preliminary study carried out on a phantom model [21]. With respect to the data collected in the experiments on phantom, the *in vivo* results present significant differences because of the intrinsic variability of real tissues. Such a variability introduces a complexity in the shape of the signals detected by the FBG during the needle penetration, as it is possible to notice in Fig. 9.

Biomedical Optics EXPRESS

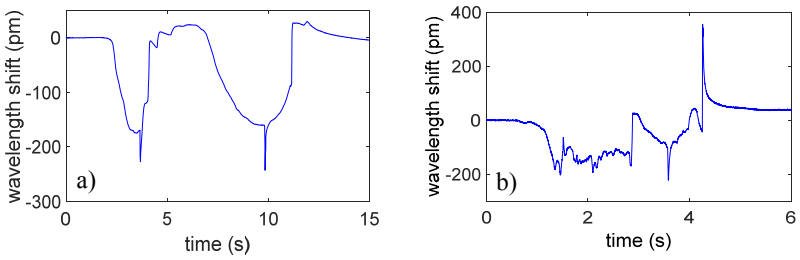

Fig. 9. Comparison between wavelength shifts measured with the Hytrel coated probe in (a) a phantom and (b) porcine model in the space L6/L7.

Although the great unpredictability observed, the device with the HCP is able, also *in vivo*, to reliably detect the force drop that is uniquely associated to the ES placement. In fact, the other force drops perceived by the probe (false positive) can be discriminated via a simple detection algorithm. Regarding the PCP, although several attempts have been made, no signal features of interest have been recorded. The different behavior is related to the (mechanical) properties of the coating materials. Hytrel is an excellent strain amplifier, which amplifies the axial deformations caused by the needle advancement into the tissues. PEEK instead, is characterized by an excellent mechanical robustness; during the advancement into the pig back the PCP remains rigid, puncturing the tissue without undergoing significant compressions.

The methodology associated to our device is familiar to the anesthesiologists and it does not alter their manual skill. In fact, the physicians insert the needle into the connective tissue and wait until a stable baseline is settled; then, the needle is advanced toward the ES while monitoring the signal evolution. When the fingerprint related to ES achievement occurs, the needle advancement is stopped and the fiber can be easily and safety removed. Successively, the anesthetic can be administered (eventually by means of a catheter). It is important to underline that our device aims to *assist* the clinicians during the needle placement into the ES; this means that it does not replace the clinicians through a full automatic decision-making algorithm, which, on the contrary, still maintain and exercise their discretion, thus having the last word in determining the success of the procedure. The proposed methodology requires a single operator, which advances the needle with both hands, without using cumbersome instrumentations. Our device has been developed only to meet the anesthesiologists need for EA, that is a sort of on/off indication that the needle tip is correctly placed inside the ES. For this specific application, our device aims to provide a reliable stand-alone measurement, without the aid of supporting imaging systems. The use of our device (and more appropriately the associated technique) can be in principle extended to other medical procedures requiring needle guidance in specific biological spaces, such as pleural drainage catheter placement and intra-articular (knee, hip, shoulder, exc.) injection, providing that assistive calibration by imaging techniques is performed. For these applications, evaluating force vs. time features at each tissue interface simultaneously with X-ray/ultrasound/MRI/CT imaging could help the clinicians in performing these procedures in a more accurate way.

Overall, this study provides only preliminary indication about the potential offered by our system as a suitable technique to localize the ES. Follow-up *in vivo* studies at other vertebral levels and in multiple subjects are necessary to perform a statistical analysis, and claim a robust system that can work in the real application. Future studies are devoted to solve the issues related to the weak biocompatibility of the fiber probe (Hytrel coating) and the possible fiber tip breakage during the needle insertion. To this aim, we are currently developing an optimized version of our optical fiber probe, where the FBG is integrated inside a standard epidural catheter, which on its turn is inserted inside the needle. Epidural catheters are characterized by the fact that their distal tip is closed (drug is administered via the holes present on the lateral surface) so that the FBG can be locked in position when it goes in

Biomedical Optics EXPRESS

contact with the closed catheter tip. This new configuration is useful to avoid any physical contact between the optical fiber probe and the human tissues. At the same time, in the accidental case of fiber breakage, the fiber glass shards remain inside the catheter and they do not disperse into the body.

Moreover, the integration of the FBG inside the epidural catheter could open the way to monitor the catheter placement inside the epidural space. Actually, in most of the epidurals, the drug injection is made by means of the catheter that is passed through the needle and, it is left in place inside the patient back once that the needle is then taken out [29]. However, during the advancement, the catheter might deviate from its straight course (desired trajectory) and bend in such a way that it fails to provide adequate analgesia. We expect that, thanks to the catheter sensorization, by monitoring the intensity of the FBG back-reflected signal, it could be possible to detect and prevent catheter bending events which are the major cause of failed epidurals [29].

5. Conclusion

In this *in vivo* swine study, we have evaluated the performances of a needle guidance system for EA. The developed device essentially consists of a special coated FBG, integrated inside the needle lumen able to measure in real time the force experienced by the needle tip during penetration through different tissues. Hytrel and PEEK coated FBGs have been tested. Experiments revealed that only the first one allows to effectively identify the ligament flavum/ES boundary. The ES placement is associated with a strong force drop, (i.e. the same that physicians perceive with the aim of the LOR syringe) that is one order of magnitude higher than all the other drops registered during penetration. Although *in vivo* measurements revealed considerable tissues variability, our method is specific and allows to effectively discriminate between ES and the biological layers that precede it, excluding false positive events. Overall, the methodology related to our device is familiar to anesthesiologists and can be performed without resorting to imaging systems. Although here demonstrated for ES localization, our results set the stage for new optical Lab-in-a-Needle systems for guiding instruments or devices towards biological spaces of the human body.

Disclosures

The authors declare that there are no conflicts of interest related to this article.

References

1. A. H. White, R. Derby, and G. Wynne, "Epidural injections for the diagnosis and treatment of low-back pain," Spine **5**(1), 78–86 (1980).
2. K. Arendt and S. Segal, "Why epidurals do not always work," Rev. Obstet. Gynecol. **1**(2), 49–55 (2008).
3. H. Elsharkawy, A. Sonny, and K. J. Chin, "Localization of epidural space: A review of available technologies," J. Anaesthesiol. Clin. Pharmacol. **33**(1), 16–27 (2017).
4. T. J. M. Lechner, M. G. F. van Wijk, A. A. J. Jongenelis, M. Rybak, J. van Niekerk, and C. J. M. Langenberg, "The use of a sound-enabled device to measure pressure during insertion of an epidural catheter in women in labour," Anaesthesia **66**(7), 568–573 (2011).
5. O. Ghelber, R. E. Gebhard, S. Vora, C. A. Hagberg, and P. Szmuk, "Identification of the Epidural Space Using Pressure Measurement with the Compuflo Injection Pump-A Pilot study," Reg. Anesth. Pain Med. **33**(4), 346–352 (2008).
6. P. Y. Lee, C. C. Huang, and H. K. Chiang, "Implementation of a novel high frequency ultrasound device for guiding epidural anesthesia - in vivo animal study," in *IEEE International Ultrasonics Symposium* (IEEE, 2013), 2049–2052.
7. G. Ameri, J. Son, J. Liang, F. S. Foster, S. Ganapathy, and T. M. Peters, "Development of a high frequency single-element ultrasound needle transducer for anesthesia delivery," Proc. SPIE **10139**, 101390S (2017).
8. C. K. Ting, M. Y. Tsou, P. T. Chen, K. Y. Chang, M. S. Mandell, K. H. Chan, and Y. Chang, "A New Technique to Assist Epidural Needle Placement: Fiberoptic-Guided Insertion Using Two Wavelengths," Anesthesiology **112**(5), 1128–1135 (2010).
9. W. C. Kuo, M. C. Kao, K. Y. Chang, W. N. Teng, M. Y. Tsou, Y. Chang, and C. K. Ting, "Fiber-needle Swept-source Optical Coherence Tomography System for the Identification of the Epidural Space in Piglets," Anesthesiology **122**(3), 585–594 (2015).

Biomedical Optics EXPRESS

10. W. C. Kuo, M. C. Kao, M. Y. Tsou, and C. K. Ting, "In vivo images of the epidural space with two- and three-dimensional optical coherence tomography in a porcine model," PLoS One **12**(2), e0172149 (2017).
11. Z. Ding, Q. Tang, C. P. Liang, K. Wu, A. Sandlerc, H. Li, and Y. Chen, "Imaging Spinal Structures With Polarization-Sensitive Optical Coherence Tomography," IEEE Photonics J. **8**(5), 1–8 (2016).
12. P. Roriz, L. Carvalho, O. Frazão, J. L. Santos, and J. A. Simões, "From conventional sensors to fibre optic sensors for strain and force measurements in biomechanics applications: A review," J. Biomech. **47**(6), 1251–1261 (2014).
13. Y. L. Park, K. Chau, R. J. Black, and M. R. Cutkosky, "Force sensing robot fingers using embedded fiber Bragg grating sensors and Shape Deposition Manufacturing," in *Proceedings of the IEEE International Conference on Robotics and Automation* (IEEE, 2007) pp. 1510–1516.
14. L. Zhang, J. Qian, Y. Zhang, and L. Shen, "On SDM/WDM FBG sensor net for shape detection of endoscope," *in Proceedings of IEEE International Conference on Robotics and Automation* (IEEE, 2005) pp. 1986–1991.
15. R. J. Roesthuis, M. Kemp, J. J. van den Dobbelsteen, and S. Misra, "Three-dimensional needle shape reconstruction using an array of Fiber Bragg Grating sensors," IEEE/ASME Trans. Mechatron. **19**(4), 1115–1126 (2014).
16. J. S. Kim, J. Guo, M. Chatrasingh, S. Kim, and I. Iordachita, "Shape determination during needle insertion with curvature measurements," *in Proceedings of IEEE/RSJ International Conference on Intelligent Robots and Systems* (IEEE, 2017), pp. 201–208.
17. R. Seifabadi, E. E. Gomez, F. Aalamifar, G. Fichtinger, and I. Iordachita, "Real-time tracking of a bevel-tip needle with varying insertion depth: Toward teleoperated MRI-guided needle steering," *in Proceedings of IEEE International Conference on Intelligent Robots and Systems* (IEEE, 2013) pp. 469–476.
18. S. Elayaperumal, J. H. Bae, D. Christensen, M. R. Cutkosky, B. L. Daniel, R. J. Black, J. M. Costa, F. Faridian, and B. Moslehi, "MR-compatible biopsy needle with enhanced tip force sensing," in World Haptics Conference (IEEE, 2013) pp. 109–114.
19. J. H. Bae, C. J. Ploch, M. A. Lin, B. L. Daniel, and M. R. Cutkosky, "Display of needle tip contact forces for steering guidance," in Haptics Symposium (IEEE, 2016) pp. 332–337.
20. Y. L. Park, S. Elayaperumal, B. Daniel, S. C. Ryu, M. Shin, J. Savall, R. J. Black, B. Moslehi, and M. R. Cutkosky, "Real-time estimation of 3-D needle shape and deflection for MRI-guided interventions," IEEE/ASME Trans. Mechatron. **15**(6), 906–915 (2010).
21. B. Carotenuto, A. Micco, A. Ricciardi, E. Amorizzo, M. Mercieri, A. Cutolo, and A. Cusano, "Optical Guidance Systems for Epidural Space Identification," IEEE J. Sel. Top. Quantum Electron. **23**(2), 1–9 (2017).
22. K. O. Hill and G. Meltz, "Fiber Bragg grating technology fundamentals and overview," J. Lightwave Technol. **15**(8), 1263–1276 (1997).
23. D. Johnson, "Novel Optical Fibers-Draw-tower process creates high-quality FBG arrays," Laser Focus World **48**(10), 53 (2012).
24. S. Fakirov, *Handbook of condensation thermoplastic elastomers* (John Wiley & Sons, 2006).
25. B. J. Lambert, F. W. Tang, and W. J. Rogers, *Polymers in Medical Applications* (iSmithers Rapra Publishing, 2001).
26. S. M. Kurtz, *PEEK Biomaterials Handbook* (William Andrew Publishing, 2011).
27. I. V. Panayotov, V. Orti, F. Cuisinier, and J. Yachouh, "Polyetheretherketone (PEEK) for medical applications," J. Mater. Sci. Mater. Med. **27**(7), 118 (2016).
28. Y. Wang, B. L. Tai, H. Yu, and A. J. Shih, "Silicone-based tissue-mimicking phantom for needle insertion simulation," J. Med. Device. **8**(2), 021001 (2014).
29. J. Hermanides, M. W. Hollmann, M. F. Stevens, and P. Lirk, "Failed epidural: causes and management," Br. J. Anaesth. **109**(2), 144–154 (2012).